SCIENCE CHINA
Information Sciences

• RESEARCH PAPER •

March 2023, Vol. 66 132301:1–132301:9
https://doi.org/10.1007/s11432-022-3499-4

Diverse terahertz wavefront manipulations empowered by the spatially interleaved metasurfaces

Jitao LI[1,3†], Zhen YUE[1†], Jie LI[1], Chenglong ZHENG[1], Silei WANG[1], Mengyao LI[1], Yating ZHANG[1*], Yan ZHANG[2*] & Jianquan YAO[1*]

[1]*School of Precision Instruments and Opto-Electronics Engineering, Tianjin University, Tianjin* 300072*, China;*
[2]*Department of Physics, Capital Normal University, Beijing* 100048*, China;*
[3]*College of Optoelectronic Engineering, Chengdu University of Information Technology, Chengdu* 610225*, China*

Received 17 January 2022/Revised 24 March 2022/Accepted 23 May 2022/Published online 16 February 2023

Abstract Optical metasurfaces have advanced approaches for manipulating light information in the spatial domain, in which the spatially interleaved metasurfaces demonstrate the ability to manipulate a more complex wavefront of light than metasurfaces without the spatial interleaving. The potential of the spatially interleaved metasurfaces has not been fully exploited. In this paper, we design the spatially interleaved terahertz (THz) metasurfaces based on the ingenious spatial interleaving principles to develop the diverse THz wavefront manipulations. Four functions are performed, including the orbital angular momentum (OAM) superposition of single-frequency vortex beams, the separate vortex focusing of single-frequency dual beams, the different OAM manipulations of bifrequency beams in different planes, and achromatic focusing. The demonstrated functions prove that the spatially interleaved metasurface can manipulate THz wavefront at both single frequency and bifrequency, which traditional metasurfaces cannot. This work paves the way for diverse THz wavefront manipulations.

Keywords terahertz, wavefront manipulations, metasurfaces, spatial interleaving, onformation optics

Citation Li J T, Yue Z, Li J, et al. Diverse terahertz wavefront manipulations empowered by the spatially interleaved metasurfaces. Sci China Inf Sci, 2023, 66(3): 132301, https://doi.org/10.1007/s11432-022-3499-4

1 Introduction

One of the important topics of modern micro-nano photonics research is optical metasurfaces, which can manipulate light information in the spatial domain by controlling the electromagnetic wave properties of light (including frequency [1], polarization [2, 3], amplitude, and phase [4]) and the photonic properties of light (such as orbital angular momentum (OAM) and spin angular momentum [5, 6]). Because of their exceptional light manipulation properties, optical metasurfaces with high research value have shown broad application prospects in the fields of information optics [7], quantum optics [8], and imaging optics [9–11], among others. Spatially interleaved metasurfaces have been proposed in recent years by optimizing structural design and spatial layout [12, 13]. They can be regarded as the integration of two (or more) metasurfaces without structural overlap. The spatial arrangement for the spatially interleaved metasurfaces is quite compact, which generally does not result in an increase and waste of the device's total area. According to design requirements, spatially interleaved metasurfaces may retain the original functions of the metasurfaces prior to spatial interleaving [12] but may also induce interaction (e.g., destructive or constructive interference [13]) to generate new functions. Therefore, in terms of polarization [14], phase [12–14], OAM [15], spin angular momentum [16], and multiphysical wave properties [17], the spatially interleaved metasurfaces typically have more powerful manipulation capabilities than ordinary metasurfaces.

However, according to existing reports, spatially interleaved metasurfaces are born only for the realization of specific functions. The advantages of the spatially interleaved metasurfaces cannot be fully

* Corresponding author (email: yating@tju.edu.cn, yzhang@cnu.edu.cn, jqyao@tju.edu.cn)
† Li J T and Yue Z have the same contribution to this work.

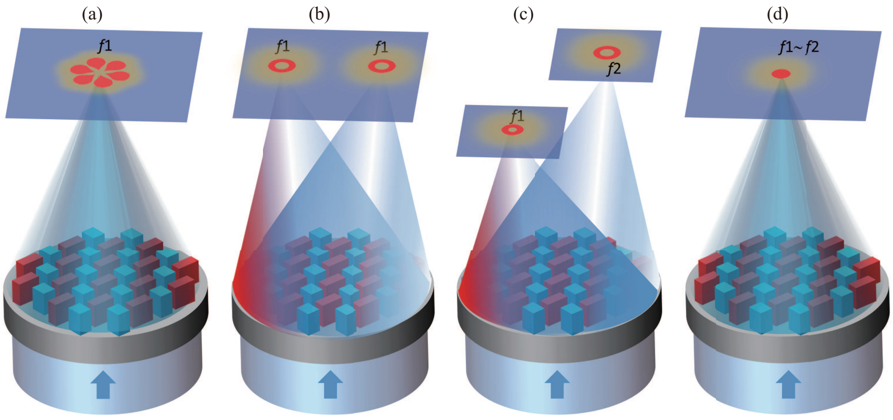

Figure 1 (Color onine) The schematic diagram for diverse THz wavefront manipulations empowered by the spatially interleaved metasurfaces. (a) An OAM superposition state at a single frequency; (b) the vortex focusing of single-frequency dual beams manipulated in the same plane; (c) the bifrequency manipulation with different OAMs and different focal planes; (d) an achromatic focusing.

utilized due to a lack of systematic research on functions. Based on the all-silicon system, we propose the spatially interleaved metasurfaces working at the terahertz (THz) region, with a systematic investigation of their functions. The spatially interleaved metasurfaces exhibit excellent capabilities for diverse THz wavefront manipulations, including OAM superposition of single-frequency vortex beams (Figure 1(a)), the separate vortex focusing of single-frequency dual beams in the same plane (Figure 1(b)), the different OAM manipulations of bifrequency beams in different planes (Figure 1(c)), and achromatic focusing (Figure 1(d)). Traditional metasurfaces cannot manipulate THz wavefronts at both single frequency and bifrequency. Therefore, the spatially interleaved metasurfaces are expected to provide a unique path for various THz wavefront manipulations.

2 Method

Three elements are proposed to realize the functions depicted in Figure 1. (1) The integration of unit cells from different metasurfaces should avoid any structural overlap to weaken harsh crosstalk; (2) to construct the metasurfaces that manipulate wavefront, a series of unit cells with a phase covering $0 \rightarrow 2\pi$ are required; (3) to construct metasurfaces with different frequency responses, two sets of unit cells operating at different frequencies are required. In detail, the high-resistance silicon (Si, $\varepsilon = 11.9$) rectangular pillar with the height of $h1 = 200$ μm is used as a meta-atom, which is on high-resistance Si substrate with $h2 = 300$ μm thickness, as shown in Figure 2(a). The period constant of unit cell is $P = 160$ μm. The Si rectangular pillar maintains a 45° angle with respect to the horizontal direction, and its length l and width w are restricted below $80 \times \sqrt{2}$ μm, as shown in Figure 2(b). Also, it is easy to see that two kinds of unit cells (as shown using red and blue, respectively) in Figure 2(c) are equivalent to that in Figure 2(a). Furthermore, two unit cells with the same geometric center can be spatially interleaved to form a new unit cell, as shown in Figure 2(d). The new unit cell maintains the original geometric center and period constant, without spatial increase and waste. Because of the size limit of l and w (below $80 \times \sqrt{2}$ μm), Si rectangular pillars of two unit cells after integration have no overlap, which can significantly weaken the malignant crosstalk between two unit cells. To complete wavefront manipulations, a series of structural parameters for l and w are scanned based on 0.8 and 1.0 THz, as shown in Figures 2(e)–(h), respectively. The six basic structures are selected, corresponding to the l and w as shown Table 1. These structures show generally equal transmission coefficients with the phase delay covering $0 \rightarrow 2\pi$, as shown in Figure 2(i) for 0.8 THz and Figure 2(j) for 1.0 THz.

All numerically simulative results were completed by employing a time-domain solver in commercial CST Microwave Studio software [18]. The periodic boundary was used in the x and y directions for a unit cell simulation, while the z direction used the open (add space) boundary. For full-size metasurface array simulation, the open boundary was used in the x and y directions, and the open (add space) boundary was used in the z direction. All samples were prepared using standard plasma etching method to etch high-resistance Si wafer (conductivity $\delta < 0.05$ S$\cdot$m^{-1}, and 500 μm thickness). Please note that the issue

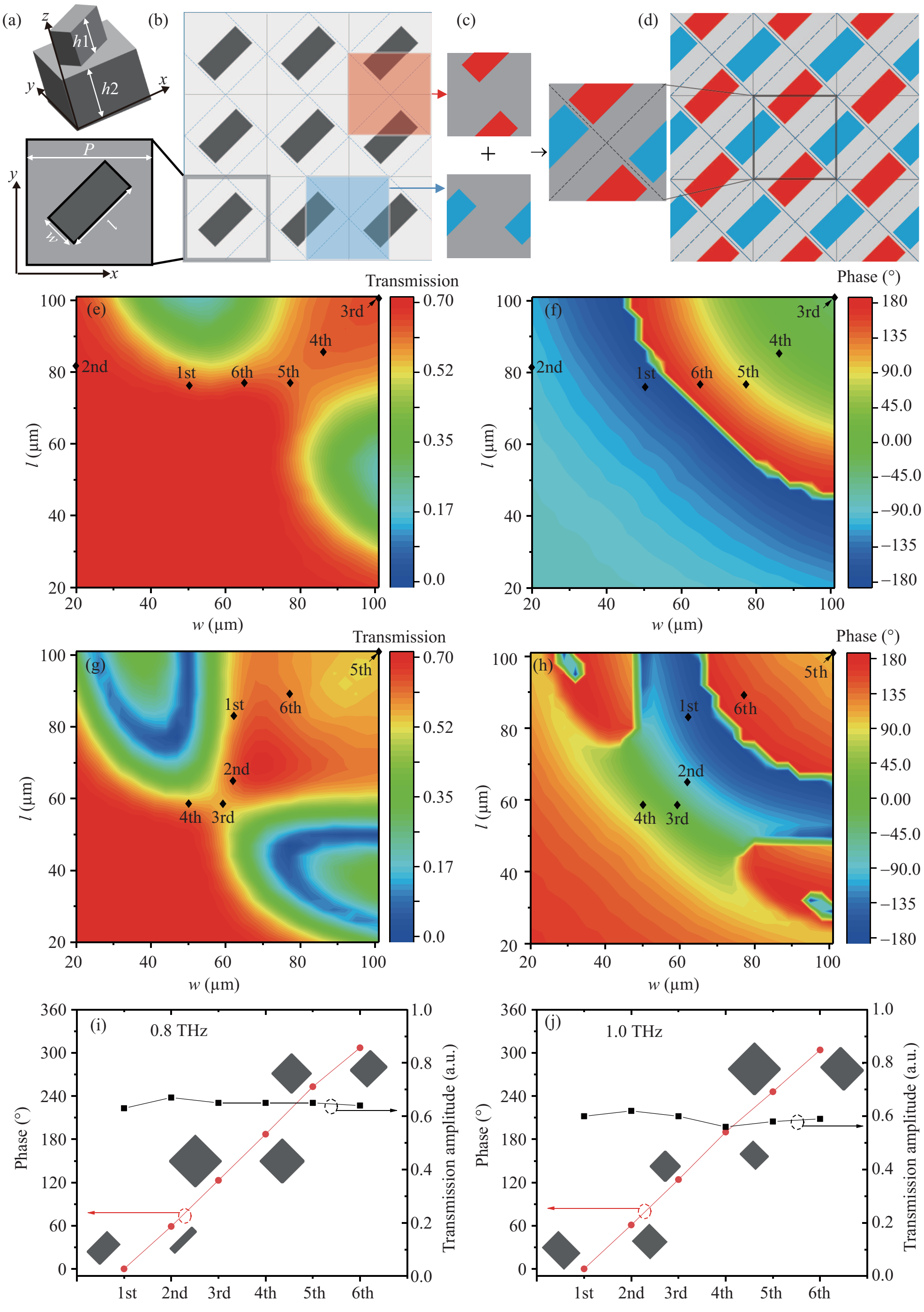

Figure 2 (Color onine) (a) The schematic meta-atom with the (b) array. (c) Two kinds of unit cells are equivalent to that in (a). (d) The integrated unit cell and array by the spatial interleaving of two unit cells in (c). Due to the size limit of l and w, Si rectangular pillars of two unit cells after being integrated have no overlap. (e), (f) Transmission amplitude and phase of the unit cell at 0.8 THz with the structural parameters (l and w) scanning, respectively. (g), (h) Transmission amplitude and phase of the unit cell at 1 THz with the structural parameters (l and w) scanning, respectively. Six units are selected for each frequency; (i) depicts the phase (red dot-line) and transmission amplitude (black dot-line) of six units at 0.8 THz; (j) depicts those of six units at 1 THz.

related to polarization is not considered in this work, and all results are based solely on the transmission and incidence of x-polarized waves. The test system is primarily based on a femtosecond laser (800 nm central wavelength) and ZnTe crystal to perform the electro-optical sampling for the THz plane wave, and then the signal post-processing module is relied upon to obtain the final map, which includes THz amplitude and phase information. For more details on the characterization method see Appendix A.

Table 1 The selected parameters l and w for structures are based on 0.8 and 1.0 THz

Frequency (THz)	Parameter (μm)	1st	2nd	3rd	4th	5th	6th
0.8	l	77	83	101	86	77	77
	w	50	20	101	86	77	65
1.0	l	83	65	59	59	101	89
	w	62	62	59	50	101	77

3 Results and discussion

A spatially interleaved metasurface may allow for more complex wavefront manipulation than a metasurface without spatial interleaving. For instance, the spatially interleaved metasurface can control an OAM vortex superposition state at a single frequency, or the separate vortex focusing on two beams of the same frequency in the same plane. Furthermore, two different frequency waves with different OAMs can be controlled in different planes, or an achromatic focusing between two different frequencies is obtained. Following that, we will demonstrate these functions.

3.1 THz wavefront manipulations at a single frequency

For a single frequency such as 0.8 THz, we use the structural parameters provided in Table 1 to first construct two metasurfaces that operate on vortex focusing with different OAMs (Figure 3(a)). The meta-atoms constructions for two metasurfaces each follows the principles of construction of two unit cells shown in Figure 2(c) (marked in red and blue, respectively; more details can be seen in Appendix B). The phase profile of each metasurface is as follows:

$$\varphi = -\frac{2\pi}{\lambda}(\sqrt{(x-x_0)^2+(y-y_0)^2+f^2}-f)+m\times\delta, \tag{1}$$

where λ is the working wavelength corresponding to 0.8 THz, (x_0, y_0) is the coordinate of the spatial focus projected onto the metasurface, and $(x_0 = 0, y_0 = 0)$ is located at the center point of the metasurface. The (x, y) is the coordinate of each point on the metasurface, and $f = 8$ mm is the focal length. The δ represents the azimuthal angle that is used as a phase factor to control the vortex of the wave [19–21] and obtained by dividing the metasurface array with a fixed phase difference under polar coordinate. The m means topological charge, which is a factor to control the OAM of te vortex beam. For two metasurfaces before incorporation, m may be the same or different. Here we choose $m = -3$ and $+3$ respectively. It should be noted that the phase profile given by (1) is a continuous value that varies with coordinates, but metaphases cannot achieve such an ideal situation. In practice, constructing a metasurface using a series of unit cells with discrete phases is a common method (see Appendix B) [22, 23].

Then, as shown in Figures 3(a) and (b), two metasurfaces can be integrated into a spatially interleaved metasurface. The performance of the interleaved metasurface is mainly affected by the interaction of units and the overall phase profile of the original metasurface; the latter (phase profile of the metasurface) determines the propagation characteristics of the far-field space beam. In general, the interaction between two units can be simply described as the sum of Jones matrices in the absence of any structural overlap and unit space sharing, thus the transmitted electric field is the superposition of the independent complex amplitudes of the two units without crosstalk. However, it should be noted that in this work, although the incorporation of two units has no overlap of Si pillars, there is still a sharing of unit space, which will generate complex crosstalk between units, resulting in the overall transmitted electric field no longer being a simple superposition of the complex amplitudes of two units (see Appendix C). Nonetheless, due to the nonoverlapping design of Si pillars, the undesired crosstalk causes only a slight attenuation of the respective properties of two metasurfaces, which is insufficient to drown out the respective far-field beam propagation properties of two metasurfaces. As a result, the overall function of the spatially interleaved metasurfaces can still be roughly described as the function superposition of two metasurfaces, as our experimental and simulation results demonstrate.

When two metasurfaces interact after incorporation, their vortex beams will obtain stable interference at the same focal point. The experimental and simulative results show the interference beam with 6-lobed electric field intensity distribution, as shown in Figures 3(c)–(f). The phase singularity causes dark fringes between lobes, indicating that the OAM superposition state is obtained in the spatially interleaved metasurface. The focusing efficiencies FE of such metasurface for experiment and simulation

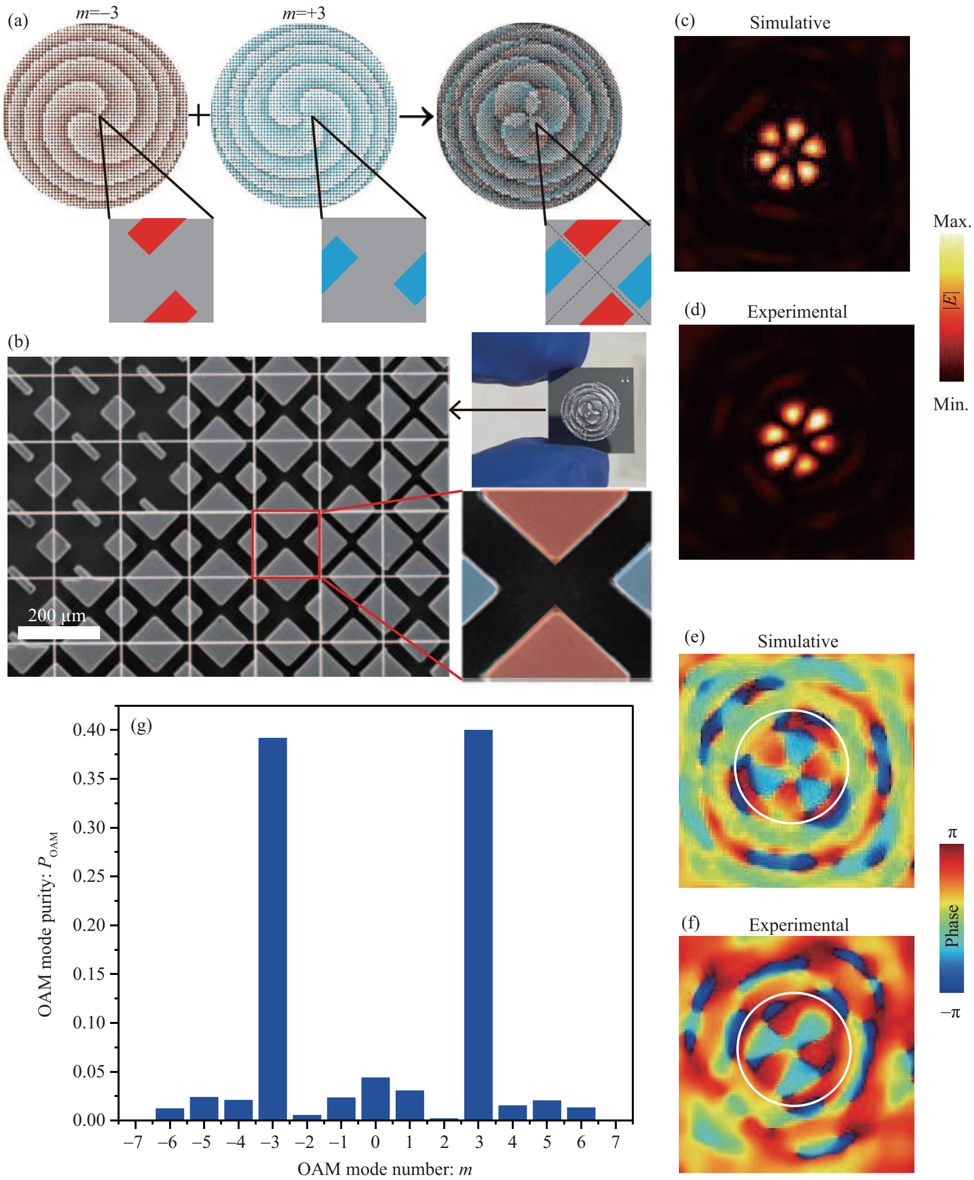

Figure 3 (Color onine) (a) The schematic diagram for an OAM superposition metasurface spatially interleaved by two metasurfaces manipulating different OAMs, corresponding to (b) the actual photograph and SEM picture, where high magnification SEM of an interleaved unit cell shows two original unit cells marked with different colors. The irregular shape may be constructed at the phase profile transition due to the inconsistent shape of two adjacent unit cells (see Appendix B). (c), (e) The simulative electric field and phase distributions in the focal plane respectively correspond to the experimental results in (d), (f). (g) The OAM mode purity chart. The working frequency is 0.8 THz.

are about 20% and 21%, respectively. FE is estimated by $\mathrm{FE} = \mathrm{Sum}(I_f)/\mathrm{Sum}(I)$, where $\mathrm{Sum}(I)$ means the total electrical field intensity incident on the metasurface, and is calculated as the integral result of electrical field intensity incident on all points of the metasurface; $\mathrm{Sum}(I_f)$ is the integral result of electric field intensity concentrated around the focus point in the focal plane, where I_f is restricted to $I_{\max}/e < I_f < I_{\max}$ ($I_{\max}$ is the maximum electrical field intensity in the focal plane) [24].

To investigate the performance of the vortex beam generators, the purity in OAM modes is calculated by linking the Fourier relationship given by [19–21]

$$A_m = \frac{1}{2\pi}\int_0^{2\pi} \psi(\delta)\mathrm{d}\delta \exp(-\mathrm{i}m\delta), \tag{2}$$

$$\psi(\delta) = \sum_{m=-\infty}^{+\infty} A_m \exp(\mathrm{i}m\delta), \tag{3}$$

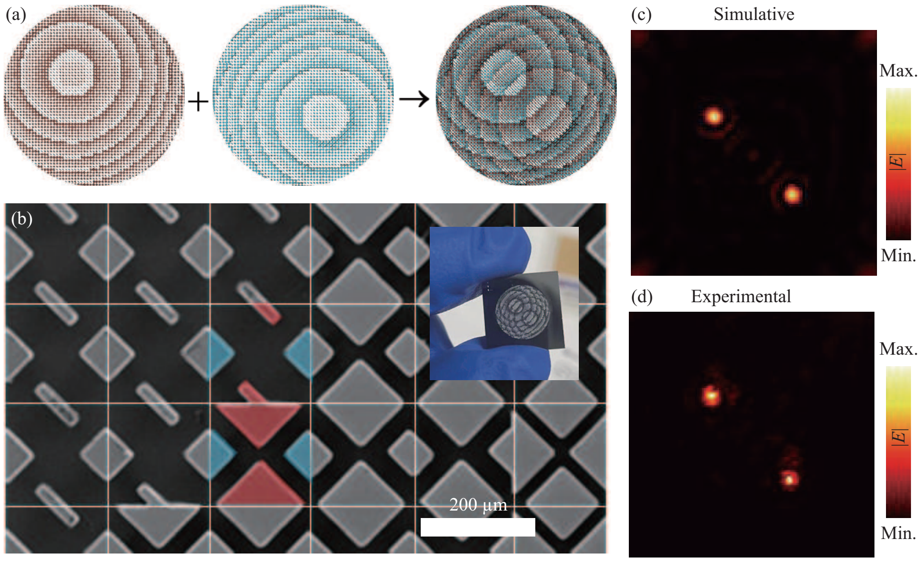

Figure 4 (Color onine) (a) The schematic diagram for a bifocal metasurface spatially interleaved by two metasurfaces with the same focal length but different focus centers. (b) SEM picture of the sample with the inset of the actual photograph, where each interleaved unit cell shows two original unit cells marked with different colors. Some irregular shapes in (b) are constructed due to the phase profile transition (see Appendix B). (c), (d) The simulative and experimental electric field distributions in the focal plane, respectively. The work frequencies for the two focus points are the same at 0.8 THz.

where A_m is angular momentum amplitude. The azimuthal angle δ is a periodic function, its Fourier conjugate. The wave function of the transmitted beam $\psi(\delta)$ is expanded by a spiral harmonic $\exp(\mathrm{i}m\delta)$, which is the characteristic wave function of OAM and is distributed periodically in the angular direction. The OAM mode purity P_{OAM} is further defined as [21]

$$P_{\mathrm{OAM}} = A_m^2 \bigg/ \sum_{n=-\infty}^{+\infty} A_n^2. \tag{4}$$

The P_{OAM} chart extracted from the OAM superposition state is depicted in Figure 3(g). It can be seen that the main modes are two vortex beams with $m = \pm 3$, and they have almost equal purity ($P_{\mathrm{OAM}} =\sim 39\%$); other modes with $m \neq \pm 3$ show low purity ($P_{\mathrm{OAM}} < 5\%$) compared with the main modes, which is well corresponded to our design.

Figure 3 depicts the superposition interference of the THz field, in which two metasurfaces manipulate wave beams in the same spatial directions prior to incorporation. Now, two metasurfaces are designed to control wave beams in different spatial directions before incorporation. As previously stated, the weak crosstalk between units is insufficient to drown out the respective far-field beam propagation properties of the two metasurfaces. As a result, the spatially interleaved metasurface may maintain the far-field beam of each metasurface (before incorporation) pointing in different spatial directions. To demonstrate this function, we design a metasurface that is spatially interleaved by two metasurfaces (same work frequency at 0.8 THz) with the same focal length but different focal centers, as shown in Figures 4(a) and (b). Each metasurface phase profile follows (1), where the coordinate of the spatial focus projected onto the metasurface is set to deviate from the metasurface center, namely $(x_0, y_0) \neq (0, 0)$. For the convenience of comparison, two focal points are designed with a π-rotation symmetry, and $m = 0$ is set to perform pure focusing. The electric field distributions show that the two beams are separated in space without superimposing, and the energy is respectively concentrated to two focal points in the same plane, as shown in Figures 4(c) and (d) for the simulated and measured results. The focusing efficiencies of the two focal points are the same due to the symmetrical design (FE $=\sim 12\%$ for simulated results and FE $=\sim 10\%$ for measured results).

3.2 THz wavefront manipulations at bifrequency

We use the structural parameters provided in Table 1 to construct two metasurfaces that operate at 1.0 and 0.8 THz, respectively; the phase profile is given by (1). They control different OAMs of vortex beams

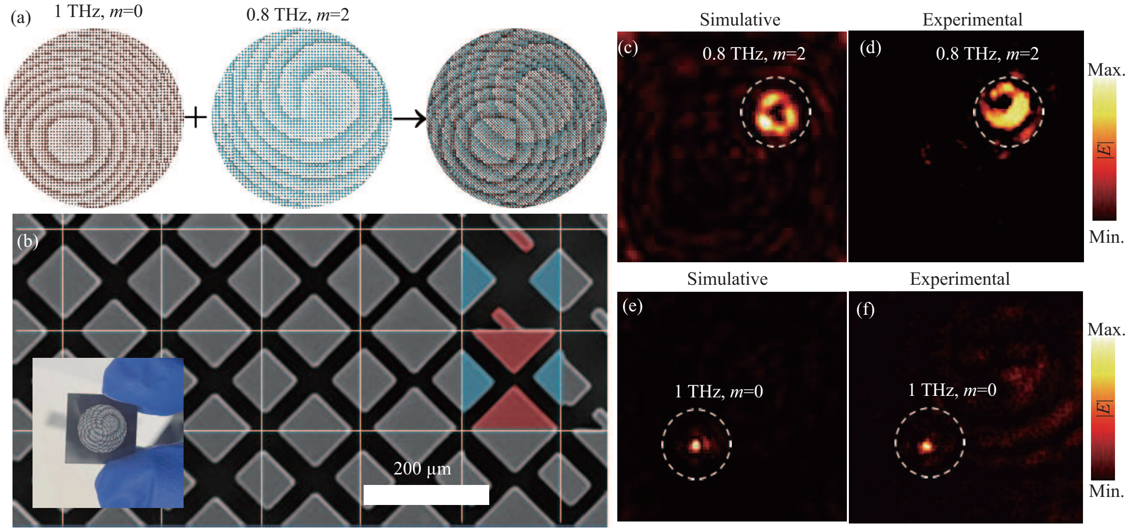

Figure 5 (Color onine) (a) The schematic diagram for a bifrequency metasurface spatially interleaved by two metasurfaces manipulating different frequencies and OAMs in different focal planes. (b) SEM picture of the sample with the inset of the actual photograph, where each interleaved unit cell shows two original unit cells marked with different colors. Some irregular shapes in (b) are constructed due to the phase profile transition (see Appendix B). (c), (e) The simulative electric field distributions were observed in different focal planes and different work frequencies, corresponding to the experimental results in (d), (f), respectively.

(respectively $m = 0$ and 2), with different focal centers and focal lengths (focal lengths are $f = 4$ and 8 mm, respectively). The meta-atoms constructions and integrations for two metasurfaces follow the same principles shown in Figures 2(c) and (d), and the final metasurface with spatial interleaving is shown in Figures 5(a) and (b). The vortex focusing electric field with an efficiency of ~ 10 % for 0.8 THz waves is successfully observed in the simulative and experimental results at the focal plane of $f = 8$ mm, and the phase singularity at the center causes the dark spot (Figures 5(c) and (d)). Furthermore, at $f = 4$ mm, a bright focusing electric field with an efficiency of $\sim 11\%$ for 1 THz wave is observed (Figures 5(e) and (f)). The results demonstrate that spatially interleaved metasurface has the potential to manipulate THz waves at bifrequency.

Furthermore, we set the focal center coordinates of the two metasurfaces to be (0, 0), with the focal lengths f of both being 8 mm, topological charges m of both being zero, and the phase profiles according to (1). Figures 6(a) and (b) depict the final metasurface with spatial interleaving. As a result of this design, the spatially interleaved metasurface will focus two THz waves of different frequencies at the same point in space, potentially forming a metalens with achromatic function in the range of 0.8–1 THz. The electric field distributions are measured at 0.8, 0.9, and 1 THz. In the same focal plane, a concentrated spot for each frequency is observed (Figure 6(c)). Further, Figure 6(d) shows the cross-sectional spatial electric field distribution of a metasurface without spatial interleaving (designed work frequency is 1 THz). It can be seen that the focal length increases with increasing frequency, indicating chromatic aberration focusing. However, as shown in Figure 6(e), the focal length for the spatially interleaved metasurface is generally unchanged in the range of 0.8–1 THz, demonstrating that an achromatic focusing is achieved. The focusing efficiencies of such a metasurface for several frequencies are approximately 21%, 19%, and 20%, for 0.8, 0.9, and 1 THz, respectively. The results show that the spatially interleaved metasurface can operate both single frequency and bifrequency waves, which is not true for the traditional metasurface without spatial interleaving.

4 Conclusion

In summary, we created a THz metasurface that is spatially interleaved by two other metasurfaces. Metasurfaces with spatial interleaving can manipulate more complex THz wavefronts than metasurfaces without spatial interleaving. The appropriate phase profile can be designed based on a series of basic structures and clever spatial interleaving principles to obtain the diverse THz wavefront manipulations at a single frequency or bifrequency. Four functions, including an OAM vortex superposition state at a single frequency, the separate vortex focusing of single-frequency dual-beam in the same plane, the

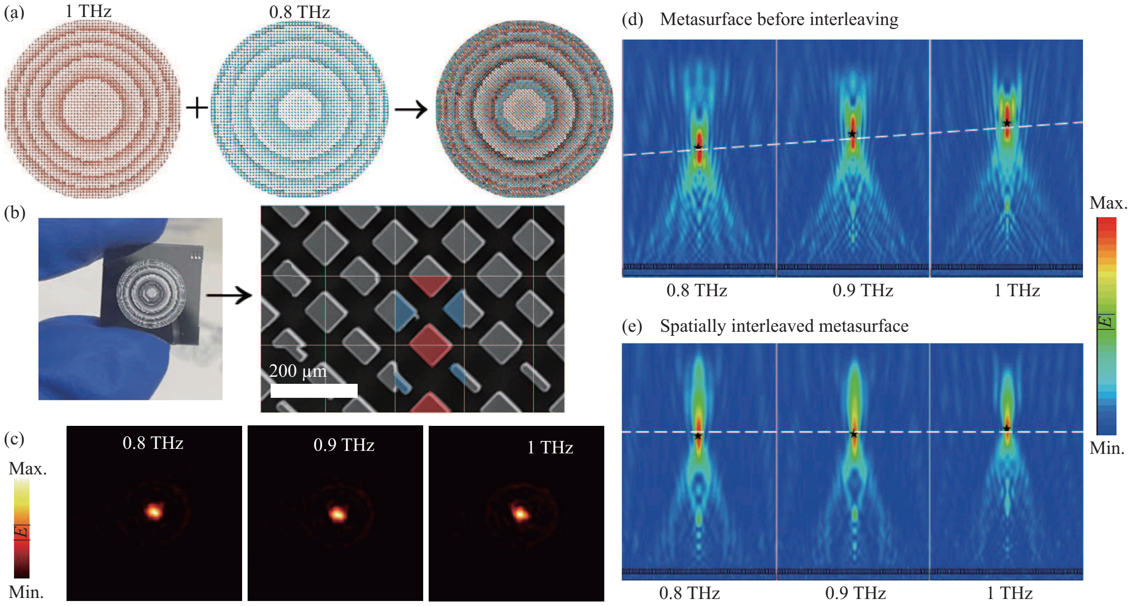

Figure 6 (Color onine) (a) The schematic diagram for an achromatic metasurface spatially interleaved by two metasurfaces manipulating different frequencies but the same focus point. (b) The actual photograph of the interleaved metasurface with the SEM picture where each interleaved unit cell shows two original unit cells marked with different colors. The phase profile transition induces some irregular shapes (see Appendix B). (c) The measured electric field distributions with different frequencies in the same focal plane, and (d), (e) the the cross-sectional electric field distributions for the original metasurface designed work frequency at 1 THz and the spatially interleaved metasurface, respectively.

different OAM controls of two different frequency waves in different planes, and the achromatic focusing, were successfully demonstrated.

Acknowledgements This work was supported by National Key Research and Development Program of China (Grant Nos. 2021YFB2800703, 2017YFA0700202), National Natural Science Foundation of China (Grant No. 61675147), and Sichuan Science and Technology Program of China (Grant No. 2021ZYD0039).

Supporting information Appendixes A–C. The supporting information is available online at info.scichina.com and link.springer.com. The supporting materials are published as submitted, without typesetting or editing. The responsibility for scientific accuracy and content remains entirely with the authors.

References

1 Balli F, Sultan M, Lami S K, et al. A hybrid achromatic metalens. Nat Commun, 2020, 11: 3892
2 Li C J, Wang C G, Yue C Z, et al. Dynamic phase assembled terahertz metalens for reversible conversion between linear polarization and arbitrary circular polarization. Opto-Electron Adv, 2022, 5: 210062
3 Rubin N A, D'Aversa G, Chevalier P, et al. Matrix Fourier optics enables a compact full-Stokes polarization camera. Science, 2019, 365: eaax1839
4 Zheng C, Li J, Yue Z, et al. All-dielectric trifunctional metasurface capable of independent amplitude and phase modulation. Laser Photon Rev, 2022, 16: 2200051
5 Jiang Z H, Kang L, Yue T, et al. A single noninterleaved metasurface for high-capacity and flexible mode multiplexing of higher-order Poincaré sphere beams. Adv Mater, 2020, 32: 1903983
6 Cao G, Xu H X, Zhou L M, et al. Infrared metasurface-enabled compact polarization nanodevices. Mater Today, 2021, 50: 499–515
7 Jin Z, Janoschka D, Deng J, et al. Phyllotaxis-inspired nanosieves with multiplexed orbital angular momentum. eLight, 2021, 1: 5
8 Kim T T, Oh S S, Kim H D, et al. Electrical access to critical coupling of circularly polarized waves in graphene chiral metamaterials. Sci Adv, 2017, 3: 1701377
9 Jin L, Dong Z, Mei S T, et al. Noninterleaved metasurface for $(2^6 - 1)$ spin- and wavelength-encoded holograms. Nano Lett, 2018, 18: 8016–8024
10 Zentgraf T. Imaging the rainbow. Nat Nanotech, 2018, 13: 179–180
11 Krasnok A. Metalenses go atomically thick and tunable. Nat Photonics, 2020, 14: 409–410
12 Yue C Z, Li C J, Li C J, et al. Terahertz metasurface zone plates with arbitrary polarizations to a fixed polarization conversion. Opto-Electron Sci, 2022, 1: 210014
13 Xu H X, Hu G, Li Y, et al. Interference-assisted kaleidoscopic meta-plexer for arbitrary spin-wavefront manipulation. Light Sci Appl, 2019, 8: 3
14 Zhou S, Shen Z, Li X, et al. Liquid crystal integrated metalens with dynamic focusing property. Opt Lett, 2020, 45: 4324–4327
15 Zheng C, Wang G, Li J, et al. All-dielectric metasurface for manipulating the superpositions of orbital angular momentum via spin-decoupling. Adv Opt Mater, 2021, 9: 2002007
16 Zhang F, Pu M, Li X, et al. All-dielectric metasurfaces for simultaneous giant circular asymmetric transmission and wavefront shaping based on asymmetric photonic spin-orbit interactions. Adv Funct Mater, 2017, 27: 1704295

17 Xu H, Hu G, Jiang M, et al. Wavevector and frequency multiplexing performed by a spin-decoupled multichannel metasurface. Adv Mater Technol, 2019, 5: 1900710
18 Zhang M, Zhang F, Li M, et al. Highly efficient amplitude modulation of terahertz fano resonance based on Si photoactive substrate by low power continuous wave. Adv Mater Technol, 2020, 5: 2000626
19 Franke-Arnold S, Barnett S M, Yao E, et al. Uncertainty principle for angular position and angular momentum. New J Phys, 2004, 6: 103
20 Jack B, Padgett M J, Franke-Arnold S. Angular diffraction. New J Phys, 2008, 10: 103013
21 Bi F, Ba Z, Wang X. Metasurface-based broadband orbital angular momentum generator in millimeter wave region. Opt Express, 2018, 26: 25693
22 Yu N, Genevet P, Kats M A, et al. Light propagation with phase discontinuities: generalized laws of reflection and refraction. Science, 2011, 334: 333–337
23 Wang Q, Zhang X, Xu Y, et al. A broadband metasurface-based terahertz flat-lens array. Adv Opt Mater, 2015, 3: 779–785
24 Zang X F, Xu W W, Gu M, et al. Polarization-insensitive metalens with extended focal depth and longitudinal high-tolerance imaging. Adv Opt Mater, 2020, 8: 1901342